Archaeological and Anthropological Sciences (2020) 12: 8
https://doi.org/10.1007/s12520-019-00964-8

ORIGINAL PAPER

Unveiling the secrets of Roman craftsmanship: mortars from *Piscina Mirabilis* (*Campi Flegrei*, Italy)

Concetta Rispoli[1] · Alberto De Bonis[1] · Renata Esposito[2] · Sossio Fabio Graziano[3] · Alessio Langella[4] · Mariano Mercurio[4] · Vincenzo Morra[1] · Piergiulio Cappelletti[1]

Received: 21 February 2019 / Accepted: 28 November 2019 / Published online: 6 January 2020

Abstract

Aim of this study is the characterisation of ancient Roman mortars collected in *Piscina Mirabilis*, located in the important geological, archaeological and historical area of the Campania Region (southern Italy): the *Campi Flegrei*. Goals of this research were (a) improving knowledge of Roman construction techniques by means of detailed microstructural and compositional examination of cementitious binding matrix and aggregates, to point out both mortar mix-design and provenance of raw materials, (b) the study of secondary minerogenetic processes and (c) comparison with modern mortars. Thanks to the permission by the former *Soprintendenza Archeologia della Campania* (authority of the archaeological heritage) current *"Parco Archeologico dei Campi Flegrei",* it was possible to collect small, non-invasive, but representative samples of mortars. Samples were studied by combined methodologies such as optical microscopy (OM) on thin sections, X-ray powder diffraction (XRPD), scanning electron microscopy analysis (SEM), energy-dispersion X-ray spectroscopy (EDS), simultaneous thermal analyses (STA) and mercury intrusion porosimetry (MIP). Results showed that local geomaterials were used in this archaeological site, as they are well consistent with the surrounding geological setting. A relevant characteristic is the hydraulicity of these mortars shown by the reaction rims of pozzolanic materials. Composition of the cementitious binding matrix is characterized by various products of reaction, including amorphous C-A-S-H gel, calcite and Al-tobermorite. Results also highlighted that porosity represents the main difference between ancient Roman mortars and modern hydraulic ones.

Keywords Ancient Roman mortars · *Piscina Mirabilis* · Mineralogical and petrographic analysis · *Campi Flegrei* · Standard hydraulic mortars

Introduction

Mortars are composite geological-based materials, consisting of hydraulic or aerial binding components, aggregates and additives and passive or active, which react with binding materials, modifying themselves during setting (Moropoulou et al. 2004).

The excellent preservation state of many Roman age manufacts demonstrates the high technological skills of these construction workers. Although evidences show that Egyptians already knew "the way" to produce "lime", it is widely acknowledged that Greeks and especially Romans used mortars as early as the third century B.C. (Collepardi 2003). Documents about the knowledge in construction fields have been passed down thanks to these civilisations. Several authors described the building art such as Cato in *De Agricola*

Electronic supplementary material The online version of this article (https://doi.org/10.1007/s12520-019-00964-8) contains supplementary material, which is available to authorized users.

✉ Concetta Rispoli
concetta.rispoli@unina.it

[1] Dipartimento di Scienze della Terra, dell'Ambiente e delle Risorse, Università di Napoli Federico II, Complesso Universitario Monte Sant'Angelo, Ed. L, Via Cintia 26, 80126 Naples, Italy

[2] Dipartimento di Studi Umanistici, Università degli Studi di Napoli Federico II, Via Porta di Massa 1, 80133 Naples, Italy

[3] Dipartimento di Farmacia, Università degli Studi di Napoli Federico II, Via D. Montesano 49, 80131 Naples, Italy

[4] Dipartimento di Scienze e Tecnologie, Università del Sannio, Via F. de Sanctis snc, 82100 Benevento, Italy

(160 B.C.), M. Vitruvius Pollio (first century B.C.) in the ten books of *De Architectura* and Pliny the Elder (23–9 A.D.) with the *Naturalis Historia* treaty.

Roman builders knew that the combination of lime with special volcanic materials (*pozzolana*) provides mortar and concrete to become hydraulic, allowing underwater hardening and increasing their mechanical strength (Collepardi 2003). The use of *pozzolana* marked a revolutionary progress in the construction technology, permitting higher speed compared with carbonation processes of slaked lime. Whether volcanic material was not available, fragments of artificial materials (ceramic fragments), possessing similar hydraulic properties of *pozzolana*, were used.

Archaeometric studies on Roman mortars were focused on the mineralogical and petrographic features of the mortar components used by Roman builders (Moropoulou et al. 2005; Silva et al. 2005; Jackson and Marra 2006; Belfiore et al. 2010; Stanislao et al. 2011; Izzo et al. 2016; Graziano et al. 2018; Di Benedetto et al. 2018). Other works based on the study of hydraulic properties of *pozzolana* detailed the processes leading to the formation of hydrated phases such as calcium silicate hydrate (CSH) and calcium aluminate hydrate (CAH) (Moropoulou et al. 2004; Jackson and Marra 2006; Fernández et al. 2010, Fichera et al. 2015; Izzo et al. 2018).

This study reports a detailed archaeometric investigation performed on nineteen mortar samples collected from pillars and walls of *Piscina Mirabilis,* the largest Roman cistern of fresh water ever built (De Feo et al. 2010). The main aims of this research were improving the knowledge of Roman construction techniques, the study of secondary minerogenetic processes affecting the investigated mortars and comparing obtained results with modern building materials.

Archaeological background

The *Fontis Augustei Aquaeductum*, original name of the Roman Serino aqueduct, (Fig. 1a) is one of the most outstanding examples of Roman hydraulic engineering plant. The aqueduct was created by the Emperor Augustus and crosses much of the Campania region ending its long course of 96 km in the Phlegraean territory in a great water cistern: *Piscina Mirabilis* (Fig. 1a, b). This structure was entirely excavated into the Neapolitan Yellow Tuff (hereafter NYT). It is 15 m high with a rectangular plan of 72 × 27 m (Fig. 1c), which could store a volume of water of approximately 12,600 m^3 (De Feo et al. 2010).

Since the outbreak of the "Grand Tour" (Borriello and D'Ambrosio 1979), it has been called *Piscina Mirabilis* and represented one of the most popular destinations for European travellers in Italy. Comparable in grandeur only to the Cistern of Istanbul, almost 500 years younger, *Piscina Mirabilis* has always been recognised as a cistern, although several interpretations were given on its use. Based on the reading of Plutarch's text, *Piscina Mirabilis* was considered as a part of the majestic villa of Lucullus. Other consolidated hypotheses reported it as a work carried out by Agrippa to supply water to the military fleet stationing in Miseno or just to connect it to the Serino aqueduct according to Emperor Nero's willingness (Borriello and D'Ambrosio 1979).

Piscina Mirabilis is divided into five long and thirteen short aisles with four rows of twelve cruciform pillars that support the barrel vault in *opus caementicium*; seventeen skylights along the side walls allowed lighting and ventilation. Walls and pillars were covered by a thick layer of cementitious clay matrix up to the water fluctuation line at 7.50 m; a basal cross-section curb prevented water stagnation (Amalfitano et al. 1990; Fig. 1c). The roof terrace, covered with a thick layer of *cocciopesto*, was communicating with the inside with a series of doors. Access to the monument was via two staircases located at opposite corners (northwest and southeast; Fig. 1d). A decantation tank (*piscina limaria:* Fig. 1e) and a 1.10 m deep drain at the centre of the cistern allowed periodic emptying and cleaning of the cistern (De Feo et al. 2010). Finally, the top openings ensured the extraction of water through machinery, which then led into the secondary distribution channels (Fig. 1f). The typical wall structure in *opus reticulatum* dates back the monument to the Augustan age.

Geological background

Piscina Mirabilis is located in the *Campi Flegrei* Area (CFA), a volcanic field immediately west of the city of Naples, also including the islands of Ischia and Procida. Its volcanic history is characterised by a great number of eruptions of mainly monogenetic edifices, which emplaced huge volumes of pyroclastic rocks and very sporadic lava flows. Two high-magnitude eruptions, the Campanian Ignimbrite (CI, 39 ka) (Fedele et al. 2008; Langella et al. 2013; Rispoli et al. 2019a, b) and the NYT (15.4 ka) (Deino et al. 2004) have emplaced a large volume of pyroclastic material deposit (Morra et al. 2010; Fig. 2).

From a petrological point of view, Phlegraean products belong to the shoshonitic series, with trachyte as the most common lithotype. Clinopyroxene, plagioclase, sanidine, biotite and magnetite are the main phases; olivine occurs only in the less evolved rocks whereas nepheline and uncommon minerals (i.e. baddeleyite, zirconolite and fluorite) can be found in the most evolved products. Accessory minerals such as zircon, brown amphibole and titanite also occur (Melluso et al. 2012).

Due to its peculiar features, *pozzolana* is the most important Phlegraean product as it has represented the main component for the production of hydraulic Roman mortars. Pozzolana is an incoherent facies of NYT formation (20–

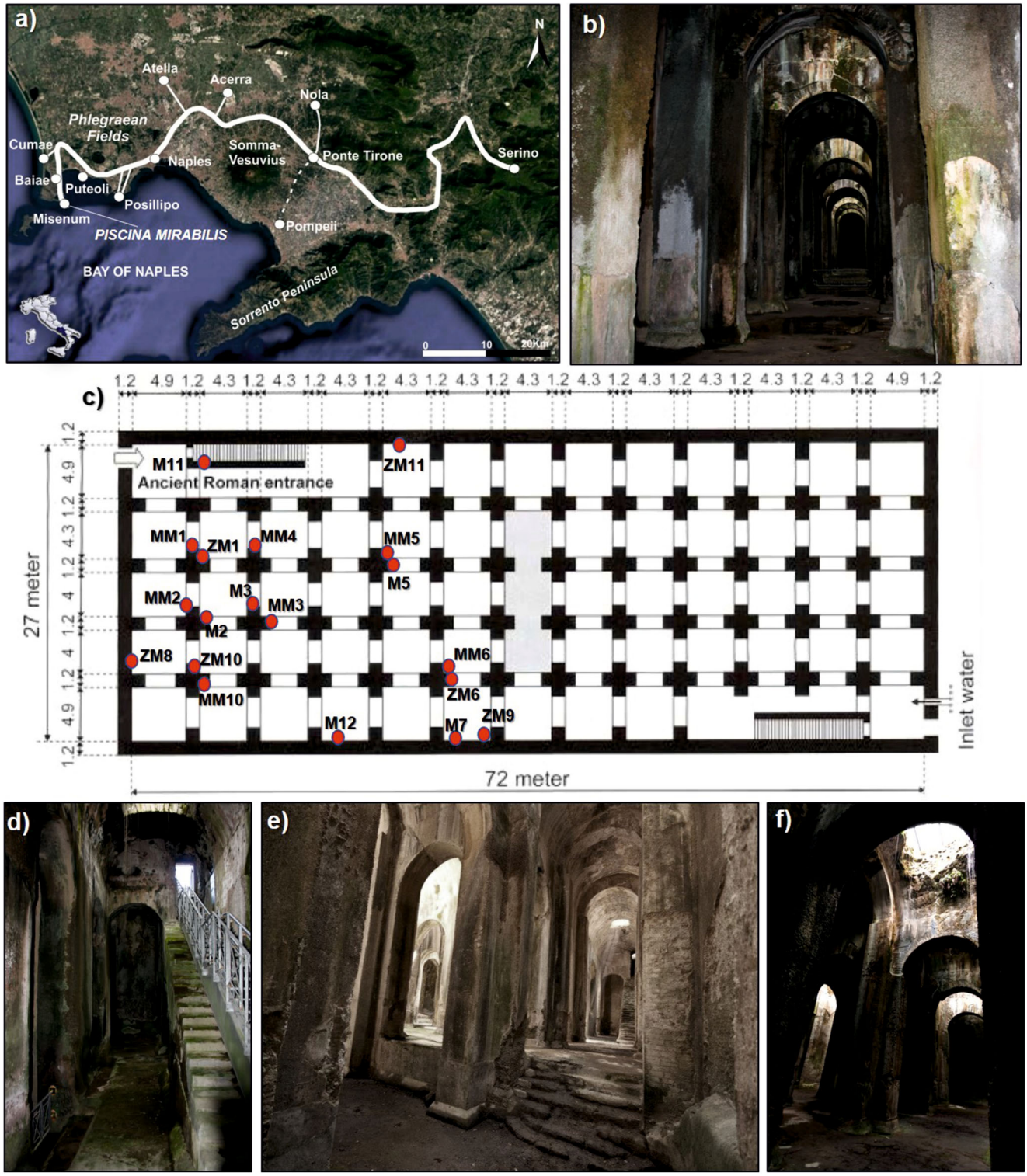

Fig. 1 **a** Route of the Augustan aqueduct from Serino to Miseno (modified after Delile et al. 2016) and location of *Piscina Mirabilis*. **b** Interior of *Piscina Mirabilis*. **c** Sketch map of the *Piscina Mirabilis* with sampling points in red (modified after Mays et al. 2013). **d** The northwest staircase (inlet water). **e** *Piscina limaria*. **f** Openings in the barrel vault

25 m thick) constituted by abundant poorly vesiculated magmatic scoriae, volcanic ash and accessory lithic fragments (Scarpati et al. 1993). The insight of the roman engineers was extraordinary: the combination of *pozzolana* with lime produced mortars and concretes able to harden underwater. A reaction of high silica and alumina *pozzolana* with calcium

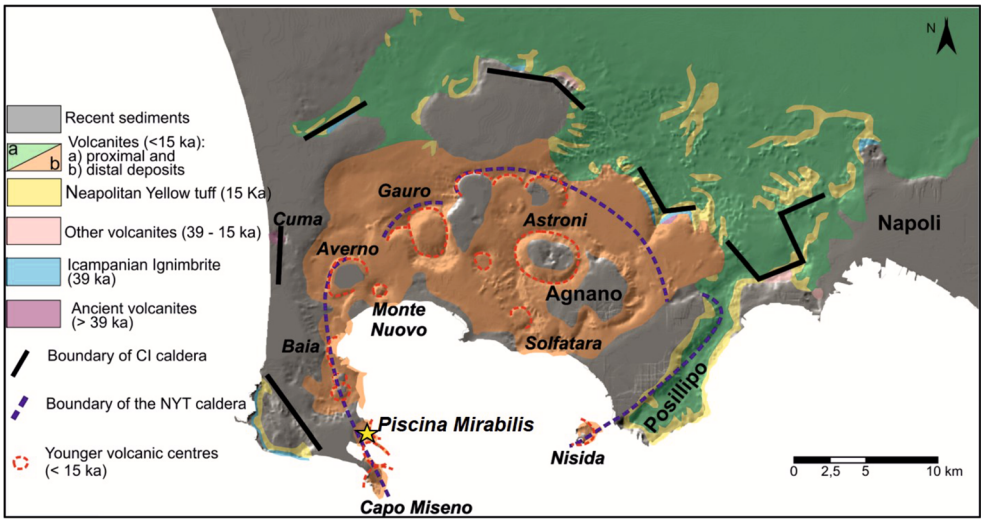

Fig. 2 Geological sketch map of *Campi Flegrei* (modified after Fedele et al. 2011)

hydroxide from lime occurred, leading to the formation of calcium aluminium silicate hydrate (C-A-S-H): the forerunners of modern cements.

Materials and methods

Nineteen mortar samples, including thirteen coating and six bedding, from pillars and walls were collected. For safety reasons, samples were collected only in one sector of the structure (Fig. 1c).

Mortar samples were sorted into three different groups (Table 1): samples from group A are coating mortars from pillars; samples from group B are coating mortars from the base of pillars and of the walls; and samples from group C are bedding mortars (Fig. 3).

Sampling collection followed specific criteria dictated by the former *Soprintendenza Archeologica della Campania* (authority of the archaeological heritage): slightest invasiveness, limited size of the samples and visual impact.

Besides, an archive research at *Soprintendenza* offices was also carried out to collect information on previous restoration works performed in the area.

The instrumental analyses were performed at DiSTAR (*Dipartimento di Scienze della Terra, dell'Ambiente e delle Risorse, Università Federico II di Napoli*), DST (*Dipartimento di Scienze e Tecnologie, Università del Sannio*) and Italcementi (HeidelbergCementGroup, Bergamo).

Petrographic analysis was carried out on thin sections using a polarized light microscope (DiSTAR-Leica Laborlux 12 pol) (Table 2). Percentage of binder, aggregate and macroporosity was determined via modal analysis using a Leica Qwin software on about 1500 points for each sample with a 10×10 counting grid. Maximum uncertainty is about 2.8% on a total amount of 1500 points (Howarth 1998).

After a careful mechanical separation carried out following the UNI-EN 11305:2009 recommendation, the mineralogical composition of binder, aggregate, ceramic fragments and neoformed phases was evaluated.

A Panalytical X'Pert Pro diffractometer (DiSTAR) equipped with a RTMS X'Celerator detector was used for X-ray powder diffraction analyses (CuKα radiation, 40 kV, 40 mA, 2θ range from 4° to 70°, equivalent step size 0.017° 2 θ, 30 s per step counting time). Panalytical Highscore Plus

Table 1 Sample list, location, typology and groups: A, coating mortars from pillars; B, coating mortars from the base of pillars and walls; and C, bedding mortars

Samples	Group	Location	Typology
MM1	A	Pillar	Coating mortar
MM2	A	Pillar	Coating mortar
MM3	A	Pillar	Concretion and coating mortar
MM4	A	Pillar	Concretion and coating mortar
MM5	A	Pillar	Concretion and coating mortar
MM6	A	Pillar	Coating mortar
MM10	A	Pillar	Coating mortar
ZM1	B	Base of pillar	Coating mortar
ZM6	B	Base of pillar	Coating mortar
ZM8	B	Base of wall	Concretion and coating mortar
ZM9	B	Base of pillar	Concretion and coating mortar
ZM10	B	Base of wall	Concretion and coating mortar
ZM11	B	Base of pillar	Coating mortar
M2	C	Pillar	Bedding mortar
M3	C	Pillar	Bedding mortar
M5	C	Pillar	Bedding mortar
M7	C	Wall	Bedding mortar
M11	C	Wall	Bedding mortar
M12	C	Wall	Bedding mortar

Table 2 Petrographic features of the samples and their microscopic modal analysis. Mineral abbreviations from Whitney and Evans (2010)

Mortars	(Group A)	(Group B)	(Group C)	M11 (Repair mortar?)
Constituents (Vol.%)				
Feldspar (Sa, Pl)	3.6	1.7	3.0	3.0
Mafic minerals (Cpx, Am, Bt)	1.4	1.0	2.0	0.7
Volcanic fragments	4.6	6.3	1.0	-
Scoriae	2.4	3.3	4.7	-
Pumice	11.0	4.3	19.0	24.0
Ceramic fragments	20.4	34.0	-	-
Sparite	2.2	0.3	-	2.3
Lime lumps	6.2	5.7	15.0	-
Micritic matric	7.4	14.0	29.3	12.7
Cryptocrystalline matrix	36.2	22.3	16.7	49.7
Voids	0.6	1.7	9.3	-
Others	4.0	5.3	-	7.7
Total points	100.0	100.0	100.0	100.0
Total binder	52.0	42.3	61.0	64.7
Total aggregate	43.4	50.7	29.7	27.7
Binder/aggregate ratio	1.2	0.8	2.1	2.3

Abbreviations: *Sa*, sanidine; *Pl*, plagioclase; *Cpx*, clinopyroxene; *Amp*, amphibole; *Bt*, biotite

3.0e with inorganic crystal structure database (ICSD) and PDF-2 database were used for phase identification.

Micro-textural observations and quantitative micro-chemical analyses were carried out using scanning electron microscopy coupled with energy dispersive spectroscopy (DiSTAR-SEM; Zeiss Merlin Vp Compact and JEOL JSM-5310; SEM/EDS: JEOL JSM-5310 coupled with an Oxford Instruments Microanalysis Unit equipped with an INCA X-act detector.

Measurements were performed with an INCA X-stream pulse processor using a 15 kV primary beam voltage, 50–100 A filament current, variable spot size, from 30.000 to 200.000 magnification, 20 mm WD and 50 s net acquisition real time. The INCA Energy software was employed using the XPP matrix correction scheme and the pulse pile up correction. The quant optimisation was carried out using cobalt (FWHM—full width at half maximum peak height—of the strobed zero = 60–65 eV). The following standards from the Smithsonian Institute and MAC (Micro-Analysis Consultants Ltd. St Ives, UK) were used for calibration: diopside (Ca), fayalite (Fe), San Carlos olivine (Mg), anorthoclase (Na, Al, Si), rutile (Ti), serandite (Mn), microcline (K), apatite (P), fluorite (F), pyrite (S), sodium chloride (Cl), benitoite (Ba) and pure vanadium (V). The Kα, Lα, Lβ or Mα lines were used for calibration, depending on the specific element.

High-resolution imaging of surface morphology (backscattered images) was generated by secondary electrons using the same instrument.

SEM-EDS analysis also allowed to measure the hydraulicity index (HI) of binder and lime lumps using spots of 10 μm on homogeneous areas. HI accounts for the (SiO_2 + Al_2O_3 + Fe_2O_3)/(CaO + MgO) ratio, as proposed by Boynton (1996).

Thermal analyses were performed on powdered bulk samples and on the < 63 μm fraction, mostly formed of binder, with the main objective of determining total hydraulicity level. The analyses were achieved by means of a Mettler Toledo TGA/SDTA 851e (Italcementi) and Netzsch STA 449 F3 Jupiter (DST–UniSannio) thermal analyser coupled with a Bruker Tensor 27 instruments and Mettler Toledo STARe SW 11.0 Netzsch Proteus 6.1.0 and Opus 7.0 software, in alumina crucibles. Mass loss from 40 to 1000 °C was evaluated at a heating rate of 10 °C/min in N_2 atmosphere (flow 60 mL/min).

Finally, pore system of samples was investigated via mercury intrusion porosimetry (MIP) on representative samples of each group selected on the basis of macroscopic and microscopic features. Analyses were performed on three fragments for each sample, and average results are reported. Two instruments (Italcementi-Thermo Fisher Scientific) were used: Pascal 140 (up to 0.4 MPa) and Pascal 240 (up to 200 MPa), which allowed to evaluate total pore volume (mm^3/g), porosity (%), bulk density (g/cm^3), apparent density (g/cm^3) and specific surface (m^2/g).

Results

Texture and optical microscopy

Coating mortars (A and B groups; Fig. 3a, b, c) show colours ranging from very pale brown (Munsell 7.5YR-7/3; Munsell

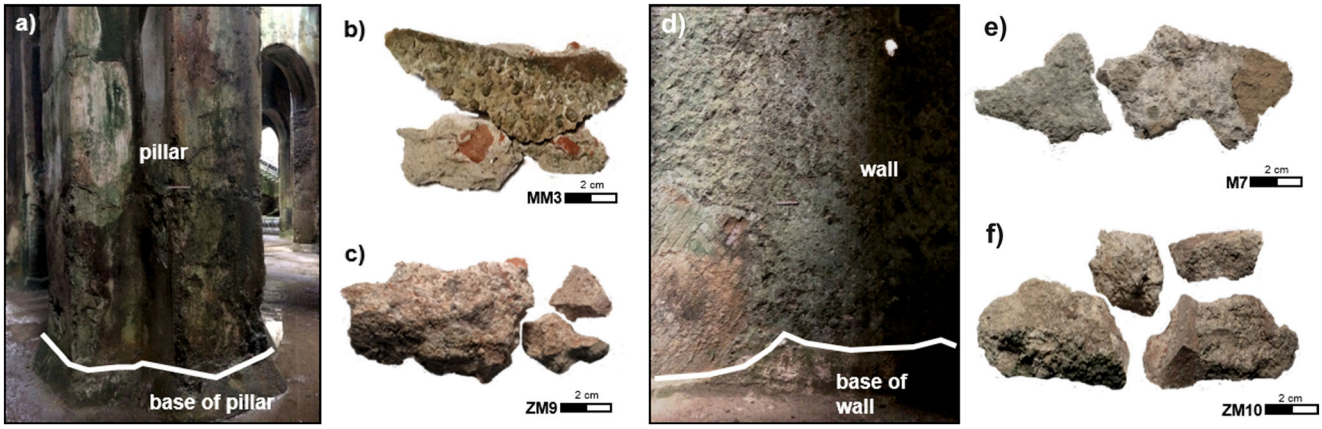

Fig. 3 **a** Pillar and base of pillar. **b** Images of coating mortars from pillar. **c** Images of coating mortars from base of pillar. **d** Wall and base of wall. **e** Images of bedding mortars from wall. **f** Images of coating mortars from base of wall

1994) to dark brown (Munsell 7.5YR-3/3; Munsell 1994) with the presence of many lime lumps. Aggregates are represented by ceramic and volcanic fragments, along with pumice varying in size from 1 to 3 cm. A concretion layer up to 3-cm thick is present on samples MM3, MM4, MM5, ZM8, ZM9 and ZM10.

Bedding mortars (C group; Fig. 3d, e, f) show pale yellow (Munsell 10YR-7/3; Munsell 1994) to light grey colour (Munsell 710YR-7/2; Munsell 1994). The aggregates consist of volcanic fragments and pumice (1 to 3 cm).

Optical microscopy shows that all mortars are characterised by lime lumps (2–1 cm), apart from sample M11. Their formation reasonably occurred during the slaking process of lime, likely due to an insufficient seasoning of calcium hydroxide and/or a low water/lime ratio (Bakolas et al. 1995; Moropoulou et al. 2005; Barba et al. 2009). Secondary calcite on pore rims and pumice vesicles also occurs.

Samples from group A are characterised by a binder with a prevailing cryptocrystalline (36.2 Vol.%; Fig. 4a) texture and a subordinate micritic one (7.4 Vol.%). Aggregate fraction is mainly composed of ceramic fragments (20.4 Vol.%; Fig. 4b), volcanic fragments (4.6 Vol.%; Fig. 4c), pumice (11.0 Vol.%) and scoriae with evident reaction rims (2.4 Vol.%). Crystal fragments such as sanidine (Fig. 4a), clinopyroxene and plagioclase also occur (5.0 Vol.%). Volcanic fragments consist of tuff fragments, due to the presence of microcrystals dispersed in an ashy matrix (de Gennaro et al. 2000).

Ceramic fragments (up to 1.5 cm) can widely vary also within the same mortar sample. Some of these fragments inclusions are mainly represented by tiny crystals of quartz and alkali-feldspar, whereas in other fragments they are characterised by a prevailing volcanic component (volcanic glass, pumice, scoriae and sanidine; Fig. 4b). In particular, ceramic matrices can be either characterized by high or low optical activity (Fig. 4b).

Concretion layers on samples MM3, MM4 and MM5 are characterised by couplets of alternating micrite and sparite laminae consisting in elongate, columnar and wedge-shaped crystals oriented at right angles to the lamination (Fig. 4d). The lamina couplets have a total thickness of 3 cm defining the layering visible in hand specimen and thin section.

Compared to group A, mortars from group B show a higher amount of ceramic fragments (34.0 Vol.%; Fig. 4f) of larger size (up to 3 cm). Volcanic fragments (6.3 Vol.%), scoriae (3.3 Vol.%), pumices (4.3 Vol.%) and crystals such as sanidine, clinopyroxene and plagioclase (2.6 Vol.%) were also recognised.

Also in this group, different texture, mineralogy and optical activity of the ceramic fragments were identified (Fig. 4f). Samples ZM8, ZM9 and ZM10 show alternating concretion layers (2 mm – 1 cm) of micrite and sparite (Fig. 4g).

Mortars from groups A and B are identified as *cocciopesto*, a typical building technique used in ancient Rome for the waterproof structures such as cisterns and floors (Collepardi et al. 2009).

Bedding mortars of group C are characterised by a brownish binder with micritic (29.3 Vol.%; Fig. 4h) to cryptocrystalline (16.3 Vol.%) texture. Differently from coating mortars, the aggregate of bedding mortars is poorly sorted, including pumice (19.0 Vol.%; Fig. 4h), scoriae (4.6 Vol.%), crystal fragments of clinopyroxene (Fig. 4i), sanidine, plagioclase and biotite (5.0 Vol.%; Fig. 4i) and minor volcanic fragments (1.0 Vol.%; Fig. 4l). M11 sample scatters from all the other samples of group C for a prevailing cryptocrystalline binder (49.7 Vol.%; Fig. 4m) and a subordinate micritic texture (12.7 Vol.%). Sparite grains (2.3 Vol.%) also occur in binder. Aggregates are rare and very poorly sorted; they are mostly composed of pumice (24.0 Vol.%; Fig. 4m) with evident reaction rims and crystal fragments of sanidine, with subordinate clinopyroxene and plagioclase (3.6 Vol.%). Such a different composition led us to consider sample M11 as a probable repair mortar in an advanced state of decay and related to a more recent restoration.

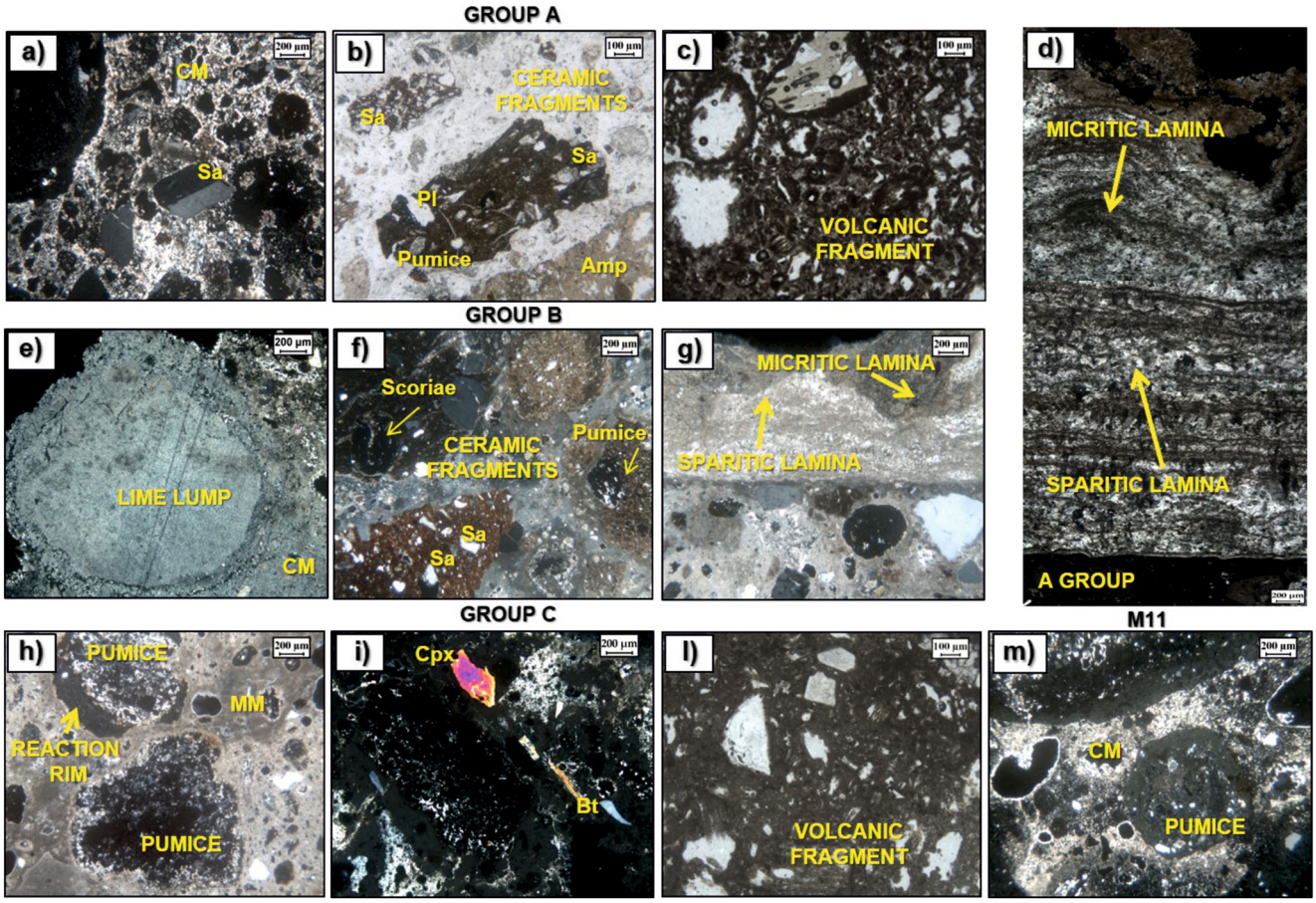

Fig. 4 Microphotographs of mortar components (in CPL: cross polarized light; PPL: plane polarized light). Abbreviations: MM micritic matrix, CM cryptocrystalline matrix, Sa Sanidine, Cpx clinopyroxene, Bt biotite, Pl plagioclase. Group A: **a** cryptocrystalline matrix and sanidine (CPL) in sample MM2. **b** Different types of ceramic fragments in sample MM10 (PPL). **c** Volcanic fragments (PPL) in samples MM5. **d** Concretion layers in sample MM4 (CPL; Rispoli 2017). Group B: **e** lime lumps (CPL) in sample ZM10. **f** Different types of ceramic fragments (CPL) in sample ZM9. **g** Concretion layers (CPL) in sample ZM9. Group C: **h** micritic matrix and pumice with reaction rims (CPL) in sample M7. **i** Volcanic fragments (PPL) in samples M5. **l** Crystal fragments of sanidine and biotite (CPL) in sample M3). **m** Cryptocrystalline matrix and pumice (CPL) in sample M11

Mineralogy

Binder, aggregates and ceramic fragments were separated from each sample according to the UNI-EN 11305:2009 and then analysed using XRPD. Results are reported in Table 3.

Binder is mainly constituted by calcite, with subordinate gypsum and Al-tobermorite $[Ca_4(Si_{5.5}Al_{0.5}O_{17}H_2)]$ $Ca_{0.2}Na_{0.1}$ $4H_2O$ (Fig. 5).

Gypsum is a common weathering product derived by the sulphation of carbonates (de Gennaro et al. 1993; Colella et al. 2017). Very interesting is the presence of Al-tobermorite, as it occurs in several samples. Al-tobermorite is a rare, hydrothermal, calcium-silicate hydrate mineral with cation exchange properties (Jackson et al. 2017); it does not occur in conventional concretes but is usually found in Roman marine concrete (Gotti et al. 2008; Stanislao et al. 2011; Jackson et al. 2012) and occasionally, in hydrothermally altered volcanic rocks such as basaltic tuff (palagonite) from Surtsey volcano, Iceland (Jackson et al. 2015, 2017).

As far as aggregates are concerned, XRPD analyses suggest that they are constituted by fragments of NYT, due to its typical zeolitic association (phillipsite, chabazite and analcime, de Gennaro et al. 1999; Colella et al. 2017), along with sanidine, pyroxene and mica as pyrogenic phases (Fig. 5b). Ceramic fragments are characterised by quartz, calcite, mica and hematite (Fig. 5c).

XRPD analyses also allowed to identify an amorphous fraction likely related to volcanic glass component (pumice and scoriae) and C–A–S–H phases (calcium–aluminium–silicate–hydrate).

Micro-morphology and chemical analysis (SEM-EDS)

SEM observations were carried out on polished thin sections of mortar fragments; EDS microanalyses of binder and lime lumps (Table 4) allowed to calculate the hydraulicity index (HI) according to Boynton's formula Boynton (1996).

Table 3 Qualitative mineralogical composition of samples, XRPD analysis. Mineral abbreviations from Whitney and Evans (2010)

Sample	Group	Main Binder Phases	Main Aggregates Phase	Main Ceramic Fragments Phases
MM1	Group A	Cal, Gp, Al-Tb	Phi, Cbz, Anl, Sa, Cpx, Pl, Mca	Qz, Cal, Sa, Cpx, Hem, Mca
MM2	Group A	Cal, Gp, Al-Tb	Phi, Cbz, Anl, Sa, Cpx, Mca	Qz, Cal, Sa, Cpx, Hem, Mca
MM3	Group A	Cal, Al-Tb	Phi, Cbz, Anl, Sa, Cpx, Mca	Qz, Cal, Sa, Hem, Mca
MM4	Group A	Cal, Al-Tb	Phi, Cbz, Anl, Sa, Cpx, Mca	Qz, Cal, Sa, Hem, Mca
MM5	Group A	Cal, Al-Tb	Phi, Sa, Cpx, Pl, Mca	Qz, Cal, Sa, Hem, Mca
MM6	Group A	Cal	Phi, Cbz, Anl, Sa, Cpx, Pl, Mca	Qz, Cal, Sa, Cpx, Hem, Mca
MM10	Group A	Cal, Al-Tb	Phi, Cbz, Anl, Sa, Cpx, Mca	Qz, Cal, Sa, Cpx, Hem, Mca
ZM1	Group B	Cal	Sa, Cpx. Mca	Qz, Cal, Sa, Hem, Mca
ZM6	Group B	Cal, Gp, Al-Tb	Phi, Cbz, Sa, Cpx, Mca	Qz, Cal, Sa, Cpx, Hem, Mca
ZM8	Group B	Cal, Gp, Al-Tb	Phi, Cbz, Sa, Cpx, Pl., Mca	Qz, Cal, Sa, Cpx, Hem, Mca
ZM9	Group B	Cal, Al-Tb	Phi, Cbz, Anl, Sa, Cpx, Mca	Qz, Cal, Sa, Cpx, Hem, Mca
ZM10	Group B	Cal, Al-Tb	Phi, Anl, Sa, Cpx, Pl, Mca	Qz, Cal, Sa, Hem, Mca
ZM11	Group B	Cal	Phi, Cbz, Sa, Cpx, Mca	Qz, Cal, Sa, Hem, Mca
M2	Group C	Cal, Gp	Phi, Cbz, Anl, Sa, Cpx, Mca	
M3	Group C	Cal	Phi, Cbz, Anl, Sa, Cpx, Pl, Mca	
M5	Group C	Cal	Phi, Cbz, Anl, Sa, Cpx, Mca	
M7	Group C	Cal, Gp	Phi, Cbz, Anl, Sa, Cpx, Pl, Mca	
M12	Group C	Cal	Phi, Cbz, Anl, Sa, Cpx, Pl Mca	
M11	Repair mortar?	Cal	Phi, Cbz, Anl, Sa, Cpx, Mca	

Abbreviations: *Cal*, calcite; *Gp*, gypsum; *Al-Tb*, tobermorite; *Phi*, phillipsite; *Cbz*, chabazite; *Anl*, analcime; *Sa*, sanidine; *Cpx*, clinopyroxene; *Pl*, plagioclase; *Mca*, mica; *Qz*, quartz; *Hem*, hematite

Chemical analyses highlighted the occurrence in the binder of newly-formed hydraulic phases (C-A-S-H) (Fig. 6a, b) and confirmed the presence of gypsum and Al-tobermorite (Al > 4%; see Supplementary Materials 1 – ESM_1) with the typical acicular habits (Stanislao et al. 2011; Jackson et al. 2017 (Fig. 6c, d). As expected, the investigated lime lumps have relatively low values of HI (< 0.1%, Fig. 7; Table 4) and thus are considered as aerial lime (quicklime) (Zawawi 2006; De Luca et al. 2015; La Russa et al. 2015). Bedding mortars showing HI values close to 0.1% should be considered as weakly hydraulic, whereas coating mortars (A and B groups) with HI ranging between 0.14 and 0.26% are moderately hydraulic mortars (Fig. 7).

SEM-EDS analysis of the volcanic aggregates confirmed the use of NYT fragments (de Gennaro et al. 1999; Di Benedetto et al. 2015; Colella et al. 2017), due to the presence

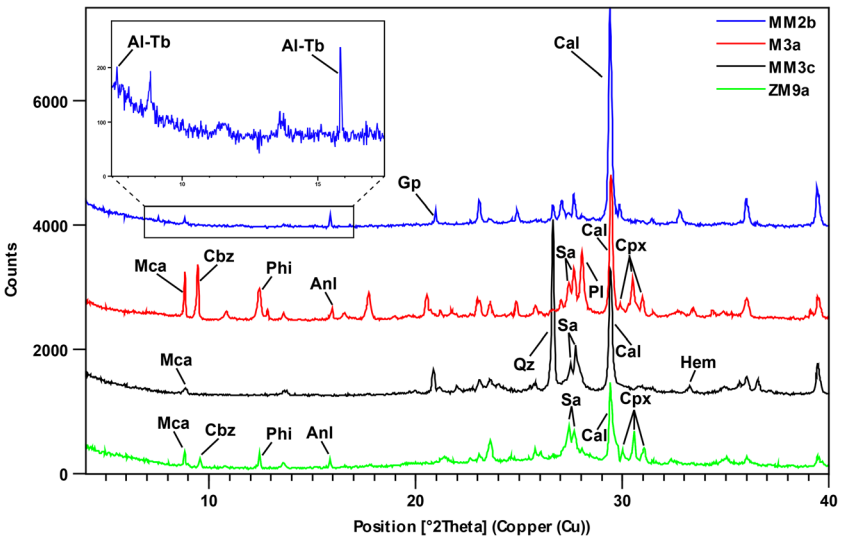

Fig. 5 XRPD patterns of selected mortars. MM2b: MM2 binder fraction (group A); M3a: M3 aggregates fraction (group C); MM3c: MM3 ceramic fraction (group A); ZM9a: ZM9 aggregates fraction (group B). Mineral abbreviations from Whitney and Evans (2010), Cal calcite, Gp gypsum, Al-Tb Al-tobermorite, Phi phillipsite, Cbz chabazite, Anl analcime, Sa sanidine, Pl plagioclase, Cpx clinopyroxene, Mca mica, Qz quartz, Hem hematite

Table 4 Average values of major oxides (wt%, recalculated to 100%, EDS), lime lumps (L) and binder (B). $SiO_2 + Al_2O_3 + Fe_2O_3$, CaO + MgO, HI (hydraulic index) are also shown

wt%	MM1L	MM1B	MM2 L	MM2 B	MM3 L	MM3 B	MM4 L	MM4 B	MM5 L	MM5 B	MM6 L	MM6 B	MM10 L	MM10 B	ZM1 L	ZM1 B	ZM6 L	ZM6 B
SiO_2	2.41	8.82	1.09	11.11	1.80	5.41	0.90	5.07	1.17	6.41	1.58	7.75	1.28	7.02	2.85	12.62	2.03	10.47
TiO_2	-	-	-	-	0.03	-	0.48	-	0.14	-	-	-	0.02	-	-	-	-	-
Al_2O_3	1.18	4.14	0.70	3.27	1.00	5.76	1.18	6.72	0.84	5.76	0.95	5.90	0.89	5.12	1.21	2.97	1.05	4.20
Fe_2O_3	0.11	0.12	-	-	0.11	-	0.15	-	0.06	-	0.04	0.10	0.10	0.17	0.23	0.36	0.03	0.09
MnO	-	-	-	-	-	-	0.18	-	-	-	-	-	0.12	-	-	-	-	-
MgO	1.65	1.41	0.29	0.71	1.20	0.07	0.61	1.33	1.32	0.07	1.88	1.30	1.17	1.20	1.68	1.02	1.74	1.41
CaO	93.41	83.14	93.66	83.54	94.86	87.75	93.14	85.16	95.86	86.75	95.12	83.54	95.66	84.97	93.14	82.02	94.27	82.15
Na_2O	0.24	0.40	0.21	0.29	0.31	0.24	-	0.39	0.21	0.24	0.09	0.27	0.25	0.29	0.33	0.28	0.15	0.37
K_2O	0.15	0.13	0.10	0.35	0.10	0.02	0.17	0.03	0.06	0.02	0.06	0.03	0.14	0.07	0.19	0.09	0.04	0.06
P_2O_5	0.05	0.42	0.15	0.07	0.19	0.22	0.51	0.31	0.19	0.22	0.01	0.02	0.06	0.25	0.07	0.22	0.03	0.02
V_2O_3	-	-	0.05	-	0.04	-	0.14	-	0.03	-	-	-	-	-	-	-	-	-
BaO	-	-	0.43	0.40	-	-	-	-	-	-	-	-	-	-	-	-	-	-
SO_3	0.72	1.12	3.17	0.07	0.10	0.48	2.34	0.85	0.02	0.48	0.24	0.96	0.31	0.79	0.23	0.15	0.63	1.05
Cl^-	0.05	0.15	0.14	0.05	0.08	-	-	0.14	0.07	-	0.03	0.13	-	0.12	0.07	0.10	0.02	0.17
F^-	0.03	0.15	-	0.13	0.18	0.05	0.19	-	0.03	0.05	-	-	-	-	-	0.17	0.01	0.01
Total	100.00	100.00	100.00	100.00	100.00	100.00	100.00	100.00	100.00	100.00	100.00	100.00	100.00	100.00	100.00	100.00	100.00	100.00
$SiO_2 + Al_2O_3 + Fe_2O_3$	3.70	13.08	1.79	14.38	2.91	11.17	2.23	11.79	2.07	12.17	2.57	13.75	2.27	12.31	4.29	15.95	3.11	14.76
CaO+MgO	95.06	84.55	93.95	84.25	96.06	87.82	93.75	86.49	97.18	86.82	97.00	84.84	96.83	86.17	94.82	83.04	96.01	83.56
HI	0.04	0.15	0.02	0.17	0.03	0.13	0.02	0.14	0.02	0.14	0.03	0.16	0.02	0.14	0.05	0.19	0.03	0.18
wt%	ZM8 L	ZM8 B	ZM9 L	ZM9 B	ZM10 L	ZM10 B	ZM11 L	ZM11 B	M2L	M2B	M3 L	M3 B	M5 L	M5 B	M7 L	M7 B	M12 L	M12 B
SiO_2	2.61	12.56	4.13	14.31	2.23	9.91	3.57	13.31	1.94	6.56	1.75	4.13	0.96	5.94	3.62	6.09	2.59	5.25
TiO_2	-	-	-	-	-	-	0.03	-	-	-	-	-	--	0.43	0.55	-	0.19	0.22
Al_2O_3	0.94	4.40	1.48	5.44	1.11	3.15	1.39	4.95	1.04	2.36	0.49	4.18	0.75	3.27	0.78	2.91	0.38	3.87
Fe_2O_3	0.48	0.06	-	0.23	0.07	0.11	0.09	0.19	0.32	0.34	0.39	0.17	0.28	-	-	-	-	0.10
MnO	-	-	-	0.14	-	-	-	0.13	-	-	-	-	-	-	-	-	-	-
MgO	0.16	1.67	0.09	1.63	1.38	1.52	0.12	1.47	0.10	1.52	0.68	0.43	0.32	0.81	3.80	0.68	2.97	1.56
CaO	93.15	79.47	90.58	76.28	94.61	83.04	93.64	78.13	94.87	85.49	95.89	87.63	96.49	86.84	90.44	88.41	93.56	88.28
Na_2O	0.07	0.55	0.60	0.57	0.22	0.45	0.28	0.59	0.02	0.49	-	0.50	0.23	0.59	0.03	0.51	0.03	0.32
K_2O	0.18	0.71	0.42	0.97	0.06	0.14	0.56	0.84	0.06	0.37	-	-	-	0.09	-	0.55	-	-
P_2O_5	-	-	-	-	0.09	0.33	-	-	-	-	-	-	-	-	0.14	-	0.04	-
V_2O_3	0.38	-	-	0.04	-	-	0.02	0.05	0.23	0.29	0.07	--	-	0.24	-	0.23	-	0.19
BaO	0.53	-	0.89	-	-	-	-	-	0.14	0.16	0.50	0.11	0.50	-	-	0.42	-	0.12
SO_3	1.42	0.42	1.59	0.37	0.08	1.10	0.20	0.34	1.15	2.17	0.12	2.57	0.36	1.74	0.62	0.18	0.24	0.09
Cl^-	0.09	-	0.23	0.02	0.10	0.13	0.10	-	0.11	0.13	0.13	-	0.13	0.06	-	-	-	-
F^-	-	0.16	-	-	0.05	0.12	-	-	0.02	0.12	-	0.27	-	-	-	-	-	-
Total	100.00	100.00	100.00	100.00	100.00	100.00	100.00	100.00	100.00	100.00	100.00	100.00	100.00	100.00	100.00	100.00	100.00	100.00
$SiO_2 + Al_2O_3 + Fe_2O_3$	4.04	17.02	5.61	19.98	3.41	13.17	5.05	18.45	3.30	9.26	2.62	8.48	1.71	9.21	4.40	9.01	2.97	9.22
CaO+MgO	93.31	81.14	90.67	77.90	95.99	84.56	93.76	79.60	94.97	87.01	96.56	88.06	96.81	87.65	94.25	89.10	96.53	89.84
HI	0.04	0.21	0.06	0.26	0.04	0.16	0.05	0.23	0.03	0.11	0.03	0.10	0.02	0.11	0.05	0.10	0.03	0.10

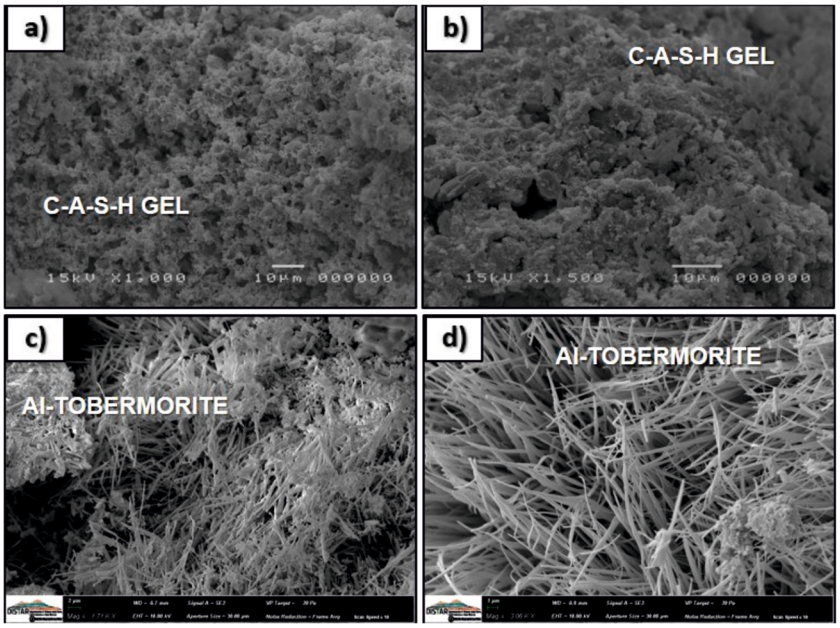

Fig. 6 SEM images of: **a** gel C-A-S-H in sample MM5; **b** gel C-A-S-H in sample ZM9; **c** Al-tobermorite in sample MM10; **d** Al-tobermorite in sample ZM6

of altered volcanic glass (Fig. 8a), prismatic crystals of phillipsite (Fig. 8b) and pseudo-cubic typically twinned rombohedral crystals of chabazite (Fig. 8c).

Chemical analyses of pumice clasts account for a trachytic composition, typical of CFA products and, in particular, of NYT (Table 5; Fig. 9).

Differential thermal and thermogravimetric analysis

Simultaneous thermal analyses were also performed to evaluate the total (binder plus aggregates) hydraulic features of mortars from *Piscina Mirabilis*. Investigated mortars (fraction < 63 μm) show a progressive loss of mass in the range 40–1000 °C (MM2 sample; Fig. 10); mass losses were generally attributed as follows (Bakolas et al. 1995; Moropoulou et al. 1995, 2004, 2005; Izzo et al. 2018):

a) mass loss up to 120 °C is related to adsorbed water;
b) mass loss in 120–200 °C temperature range is due to water from hydrated salts (i.e. gypsum);
c) mass loss from 200 to 600 °C is associated to structurally bound water (SBW) from the hydraulic compounds (i.e. C-A-S-H);
d) mass loss above 600 °C is essentially due to decomposition of carbonates.

All investigated samples are characterised by structurally bound water (SBW) and CO_2 contents typical of hydraulic mortars. In particular, the CO_2/SBW (Table 6) ratios, according to Moropoulou et al. 2005, define the samples from *Piscina Mirabilis* as highly hydraulic mortars and can be classified as natural pozzolanic mortars (Fig. 11).

Porosity

Porosity was evaluated using mercury intrusion porosimetry (MIP), according to ASTM D4404 18.

The analyses were performed on selected samples (M7 for group C, MM4 for group A, ZM8 for group B) due to the scarce amount of material available. Table 7 reports cumulative volume, bulk density, apparent density, open porosity and specific surface, whereas Fig. 12 shows the representative pore size distribution.

Relative volume curves are positively skewed and highlighted that pore radii mainly range between 5 and 100 nm. The open porosity ranges from 39.90 to 52.40 vol.% (Table 6) with unimodal and broadened shape of the cumulative pore size distribution (Fig. 12).

Comparison with standard hydraulic mortar

Roman mortars and concretes provide an outstanding example of longevity and environmental sustainability, as they were formulated with natural materials such as lime and pyroclastic rock aggregates. In order to compare the technological behaviour of these ancient products with the modern ones, an experimental standard hydraulic mortar (SHM) was prepared.

According to UNI-EN 196-1: 2005, SHM is a special type of mortar used to determine the conformity of a cement to a specific class of resistance (UNI-EN 197-1: 2011). The mix

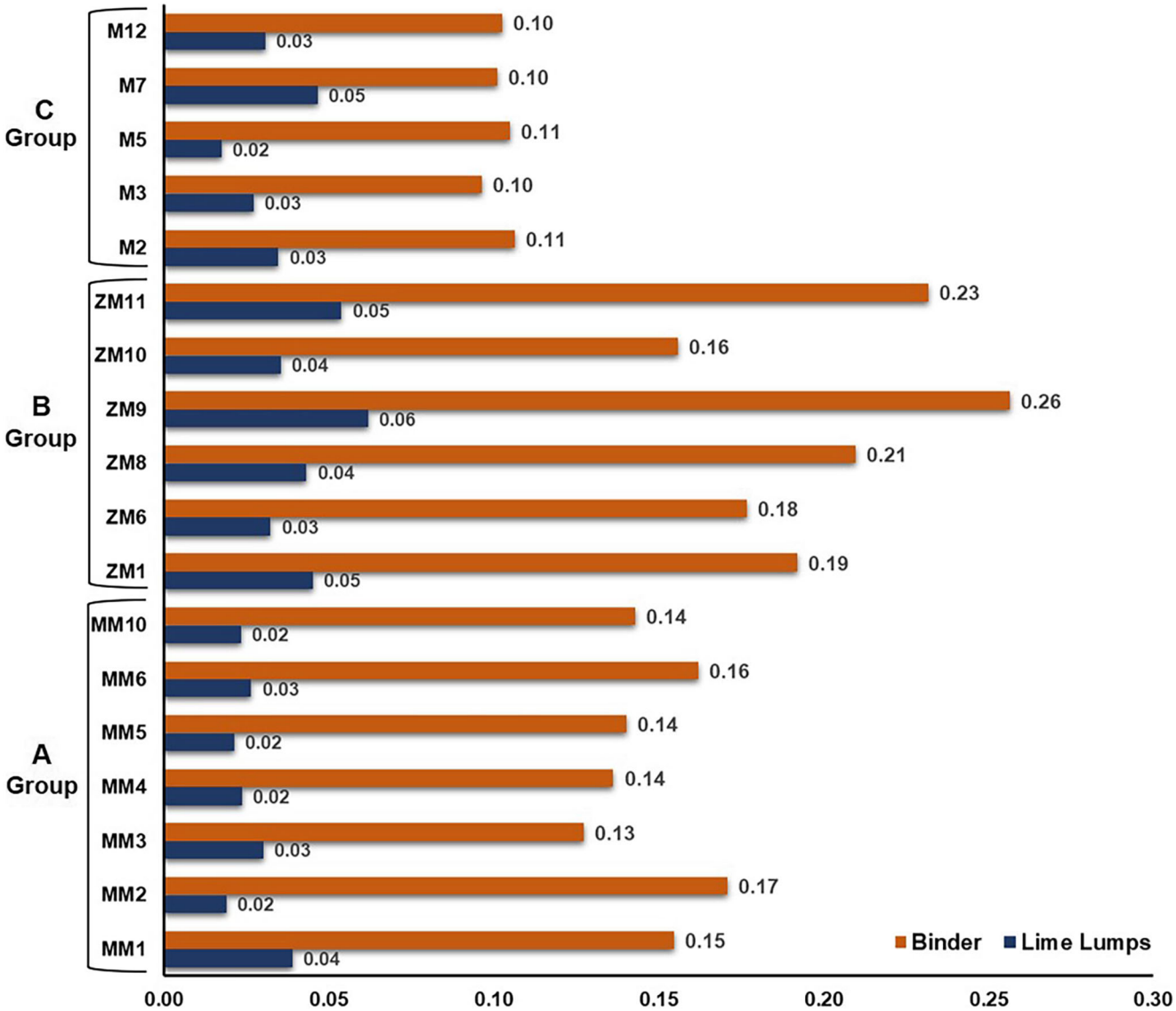

Fig. 7 Hydraulicity index (HI) for lime lumps (blue) and binder (orange) of analysed mortars

design used for SHM preparation is one part of natural hydraulic lime, three parts by mass of CEN Standard sand and one-half part of water (water/cement ratio 0.5). The above reported raw materials were mechanically mixed and then compacted in mould using a jolting apparatus. Specimens were stored in a moist atmosphere (T: 20 ± 1 °C; RH > 90%) for 24 h. Once demoulded, specimens were stored under water and, after 40 days of curing, were analysed via differential thermal and thermogravimetric analysis (DTA-TG) and MIP.

Fig. 8 SEM images of **a** altered volcanic volcanic glass (MM4 sample); **b** prismatic phillipsite crystals (M2 sample); **c** pseudo-cubic twinned chabazite crystals (MM6 sample)

Table 5 Major element concentrations of pumice fragments (wt%, recalculated to 100%, EDS). Na_2O+K_2O also shown

wt.%	MM1	MM1	MM2	MM2	MM3	MM3	MM4	MM4	MM5	MM5	MM6	MM6
SiO_2	60.10	59.95	58.59	59.27	60.57	59.97	58.41	58.40	60.40	60.48	58.92	59.86
TiO_2	0.26	0.45	0.54	0.39	0.37	0.34	0.55	0.49	0.50	0.20	0.50	0.19
Al_2O_3	18.54	18.89	18.81	18.53	18.89	18.42	18.86	19.08	18.81	18.81	18.84	18.91
Fe_2O_3	2.78	3.64	3.46	3.52	2.86	3.20	4.04	4.44	3.03	2.67	4.05	2.60
MnO	0.32	0.11	0.20	0.32	0.14	0.41	0.09		0.15	0.09	0.16	
MgO	0.32	0.38	0.85	0.35	0.33	0.37	0.49	0.77	0.31	0.27	0.63	0.42
CaO	3.52	2.63	3.20	2.84	2.27	2.40	2.88	2.89	2.06	2.02	2.66	2.53
Na_2O	4.93	3.41	3.46	3.76	4.84	5.59	3.49	4.12	5.19	4.75	3.61	5.02
K_2O	8.55	9.83	9.88	9.94	8.49	8.19	9.89	9.31	8.05	9.07	9.97	9.11
P_2O_5	-	-	0.09	-	-	0.17	0.16	0.11	-	-	-	-
V_2O_3	-	-	-	-	0.19	0.08	0.24	0.06	0.21	-	0.08	-
BaO	-	-	-	0.19	-	0.07	0.29	-	0.30	0.42	-	0.73
SO_3	-	0.14	0.04	0.17	0.14	-	-	-	0.14	0.23	-	-
Cl^-	0.68	0.57	0.88	0.71	0.91	0.79	0.61	0.78	0.86	0.99	0.58	0.64
Total	100.00	100.00	100.00	100.00	100.00	100.00	100.00	100.00	100.00	100.00	100.00	100.00
Na_2O+K_2O	13.48	13.24	13.34	13.70	13.32	13.78	13.38	13.43	13.24	13.82	13.58	14.13
wt%	ZM1	ZM1	ZM6	ZM6	ZM8	ZM8	ZM9	ZM9	ZM10	ZM10	ZM1	ZM11
SiO_2	59.75	60.97	61.82	61.84	61.14	61.41	60.46	59.63	60.21	60.88	60.97	58.52
TiO_2	0.50	0.23	0.46	0.40	0.70	0.44	0.22	0.44	0.36	0.21	0.23	0.50
Al_2O_3	18.45	18.45	18.01	18.89	18.52	18.26	18.86	18.83	18.51	19.45	18.45	19.01
Fe_2O_3	3.50	2.55	2.87	2.72	4.15	3.96	3.06	3.16	2.74	2.27	2.55	4.36
MnO	0.27	0.12	-	0.06	-	0.22	0.20	-	0.38	-	0.12	0.03
MgO	0.40	0.37	0.23	0.31	0.34	0.39	0.43	0.44	0.49	0.38	0.37	0.52
CaO	2.68	2.35	2.14	2.25	2.32	1.83	2.56	2.72	2.24	2.16	2.35	2.98
Na_2O	3.76	4.10	4.38	4.23	4.20	4.45	4.27	4.09	4.66	4.08	4.10	4.09
K_2O	9.87	9.50	9.30	8.46	8.63	8.21	9.06	9.65	9.04	9.41	9.50	9.32
P_2O_5	-	0.27	-	0.25	-	-	0.09	0.22	0.22	0.30	0.27	-
V_2O_3	-	0.09	-	-	-	-	-	-	0.15	-	0.09	0.04
BaO	-	0.07	-	-	-	0.33	0.13	-	0.20	0.04	0.0 7	-
SO_3	0.15	0.20	0.20	-	-	-	-	0.08	0.02	0.20	0.20	-
Cl^-	0.67	0.73	0.57	0.60	-	0.88	0.65	0.73	0.77	0.63	0.73	0.63
Total	100.00	100.00	100.00	100.00	100.00	100.00	100.00	100.00	100.00	100.00	100.00	100.00
Na_2O+K_2O	13.63	13.60	13.68	12.69	12.83	12.66	13.33	13.75	13.69	13.49	13.60	13.41
wt%	M2	M2	M3	M3	M5	M5	M7	M7	M11	M11	M12	M12
SiO_2	58.73	59.68	57.91	60.95	60.01	60.23	60.93	59.97	60.12	60.01	59.96	59.27
TiO_2	0.49	0.35	0.50	0.58	0.48	0.24	0.56	0.28	0.71	0.52	0.31	0.28
Al_2O_3	18.74	18.81	18.98	18.60	18.65	18.36	18.64	18.76	18.12	18.83	18.89	18.77
Fe_2O_3	3.80	3.21	4.10	2.44	2.62	4.01	2.46	3.46	3.00	2.81	3.25	2.89
MnO	0.22	-	0.16	0.26	0.27	0.11	0.23	0.40	-	0.21	0.09	-
MgO	0.45	0.42	0.73	0.31	0.53	0.39	0.44	0.31	0.53	0.29	0.27	0.69
CaO	2.70	3.01	2.76	2.09	2.92	2.16	2.23	2.34	2.26	2.40	2.05	3.12
Na_2O	4.10	4.05	3.70	4.98	3.31	4.52	4.86	4.75	5.21	5.42	4.72	3.37
K_2O	9.88	9.65	10.09	8.72	10.56	9.14	8.74	8.82	9.04	8.74	9.09	10.01
P_2O_5	-	-	0.20	0.25	-	-	0.15	-	0.20	0.12	-	0.42
V_2O_3	-	-	0.08	-	0.09	-	-	0.12	-	-	-	0.22
BaO	-	-	-	-	-	-	-	-	-	-	0.38	0.32
SO_3	0.10	0.08	0.20	-	-	-	-	-	-	-	-	-
Cl^-	0.79	0.73	0.58	0.83	0.55	0.84	0.76	0.80	0.81	0.65	0.99	0.65
Total	100.00	100.00	100.00	100.00	100.00	100.00	100.00	100.00	100.00	100.00	100.00	100.00
Na_2O+K_2O	13.98	13.70	13.79	13.70	13.87	13.66	13.60	13.56	14.24	14.16	13.81	13.38

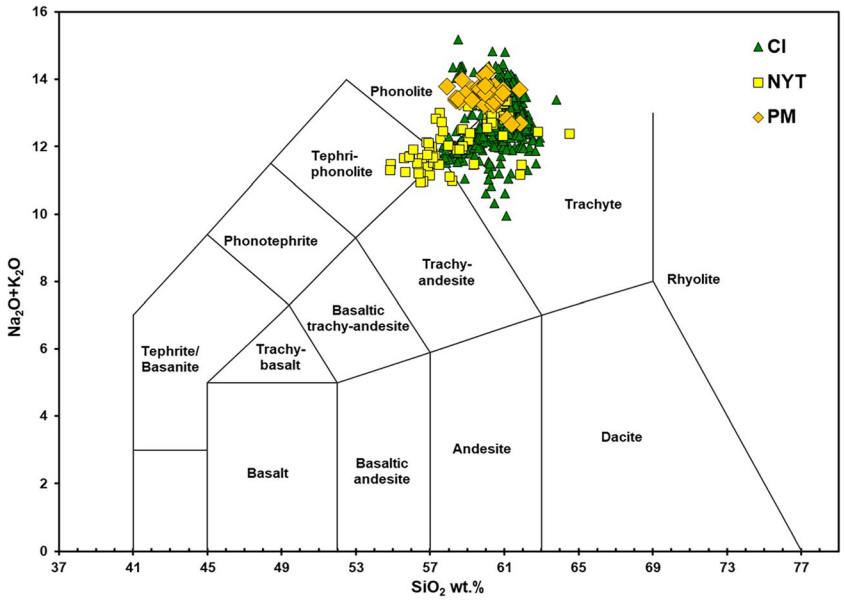

Fig. 9 Total-alkali silica (TAS) diagram (Le Bas et al. 1986) showing the composition of pumice fragments analysed in the investigated samples (PM, *Piscina Mirabilis*) and comparison with Phlegraean pumice (CI, Campanian Ignimbrite and NYT, Neapolitan Yellow Tuff; data from Morra et al. 2010 and references therein)

According to Moropoulou et al. 2005, SHM can be classified as NPM (natural pozzolanic mortar; Fig. 11); the total porosity of SHM prepared for the present research was 23.9 Vol.% with a bi-modal and broadened pore size distribution.

Comparison between Roman mortars from *Piscina Mirabilis* and SHM showed no significant differences in DTA-TG patterns, whereas MIP highlighted different values of pore radii and total porosity (Fig. 13); actually, average results of ancient Roman mortars showed a pore radius distribution between 4 and 120 nm and an open porosity ranging between 31 and 53 Vol.%; by contrast, SHM is characterized by larger pore radii (between 100 and 1000 nm) and lower values of total porosity (≈ 28 Vol.%; Fig. 13).

Discussion

Minero-petrographic, chemical and physical-mechanical analyses performed on mortars from *Piscina Mirabilis* suggested different "recipes" for the investigated samples.

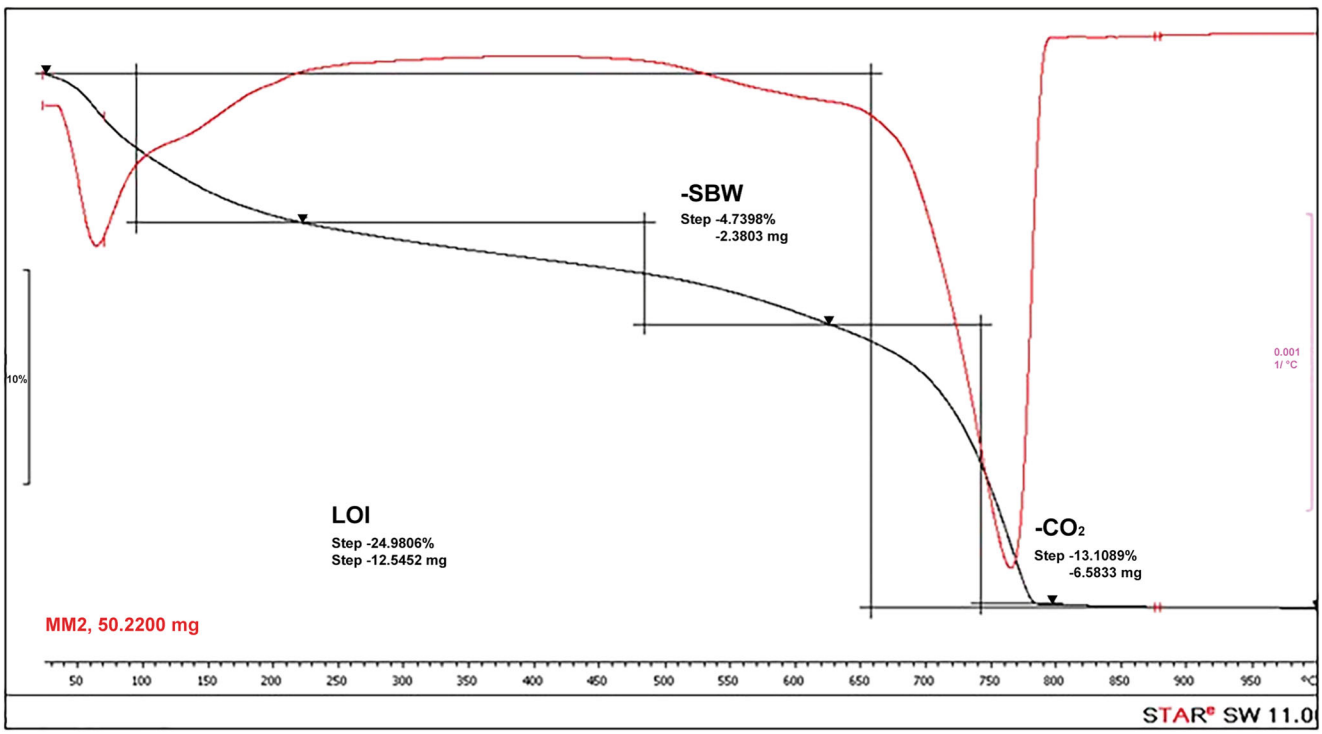

Fig. 10 DTA-TG plot of MM2 sample: dehydration of calcium silicates, aluminates hydrates and calcite decomposition are highlighted

Table 6 Thermal analysis features of investigated samples. Abbreviations: SBW structural boundary water, LOI loss on ignition

Sample	SBW%	CO_2%	CO_2/SBW	LOI
MM2 T range (°C)	4.73220–630	13.12630–800	2.77	24.98 25–1000
MM3 T range (°C)	3.96223–602	9.42602–812	2.38	18.52 25–1000
MM4 T range (°C)	5.11220–630	12.22630–783	2.39	24.25 25–1000
MM5 T range (°C)	5.29210–620	12.59620–813	2.38	23.73 25–1000
MM6 T range (°C)	4.07210–535	6.99535–814	1.72	17.69 25–1000
ZM6 T range (°C)	4.85212–660	15.38660–815	3.17	24.91 25–1000
ZM10 T range (°C)	3.42203–623	11.72623–801	3.43	20.63 25–1000
M3 T range (°C)	5.02180–621	17.77621–798	3.54	25.21 25–1000
M5 T range (°C)	4.83180–621	16.54630–810	3.42	24.35 25–1000
M11 T range (°C)	5.87210–620	7.01620–810	1.19	21.43 25–1000

As a rule, all mortars (bedding and coating) were obtained starting from a mixture of slaked lime, water and fine-grained volcanic materials. The main difference is given by the aggregate: as far as bedding mortars (C group) are concerned, aggregate was exclusively constituted by material of volcanic origin, whereas coating mortars (A and B groups) were characterised by volcanic, ceramic and carbonate aggregates.

The mix design of coating mortars is also called *cocciopesto* or *Opus signinum* by Vitruvius in his *De architectura* (*Liber* VIII): the author described this mix-design (*signinum*) useful for waterproofing tanks, thermal pools and caverns of aqueducts. Vitruvius states as follows: *Sin autem loca dura erunt aut nimium venae penitus fuerint, tunc signinis operibus ex tectis aut superioribus locis excipiendae sunt copiae. In signinis autem operibus haec sunt facienda. Uti harena primum purissima asperrimaque paretur, caementum de silice frangatur ne gravius quam librarium, calx quam vehementissima mortario mixta, ita ut quinque partes harenae ad duas respondeant.* If the soil is too hard, and there are no veins of water, we must then use cisterns made of cement, in which water is collected from roofs and other high places. The cement of the cistern thus should be constituted by the purest and roughest sand; flint should be broken in single pieces that weigh no more than a pound; lime must be mellow and mixed into mortar, using five parts of sand and two parts of lime (*De Architectura, Liber VIII*).

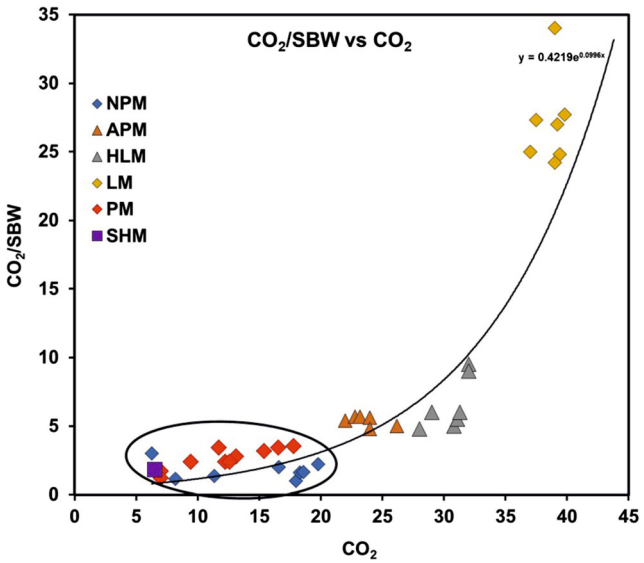

Fig. 11 CO_2/SBW vs. CO_2 diagram. Mortars from *Piscina Mirabilis* (PM, black circle); NPM natural pozzolanic mortars, APM artificial pozzolanic mortars, HLM hydraulic lime mortars and LM lime mortars from Moropoulou et al. 2005; PM *Piscina Mirabilis* mortars, SHM standard hydraulic mortar

The values of HI and thermal analyses allowed us to assess the hydraulicity of mortars. The lime lumps showed a HI lower than 0.10% which classify them as quicklime or aerial lime (Fig. 7; La Russa et al. 2015); HI of binders (0.10%–0.26%) accounts for weakly-to-moderately hydraulic materials (Zawawi 2006) as a consequence of the occurrence of materials with pozzolanic activity (ceramic and volcanic fragments). Hydraulicity is due to the reaction between silica and alumina of pozzolanic materials and lime leading to the formation of calcium and aluminium silicate hydrates, the so-called C-A-S-H phases (De Luca et al. 2015; Rispoli et al. 2016).

The hydraulicity of mortars was also confirmed by relatively high contents of structurally bound water (SBW) and CO_2, as determined by thermal analyses (Table 6); actually, their peculiar thermal behaviour is related to the presence of hydrated compounds such as C-A-S-H gel, and to the decomposition of calcite and other carbonates that usually occur between 600 and 850 °C (Izzo et al. 2018; Rispoli et al. 2019a, b). The CO_2/

Table 7 Porosimetric features (MIP) of *Piscina Mirabilis* mortars

Sample	M7	MM4	ZM8
Cumulative volume (mm^3/g)	295.86	264.35	295.33
Bulk density (g/cm^3)	1.47	1.61	1.72
Open porosity (Vol.%)	42.47	39.90	52.40
Specific Surface (m^2/g)	27.48	30.83	29.32
Apparent Density (g/cm^3)	2.56	2.70	4.97

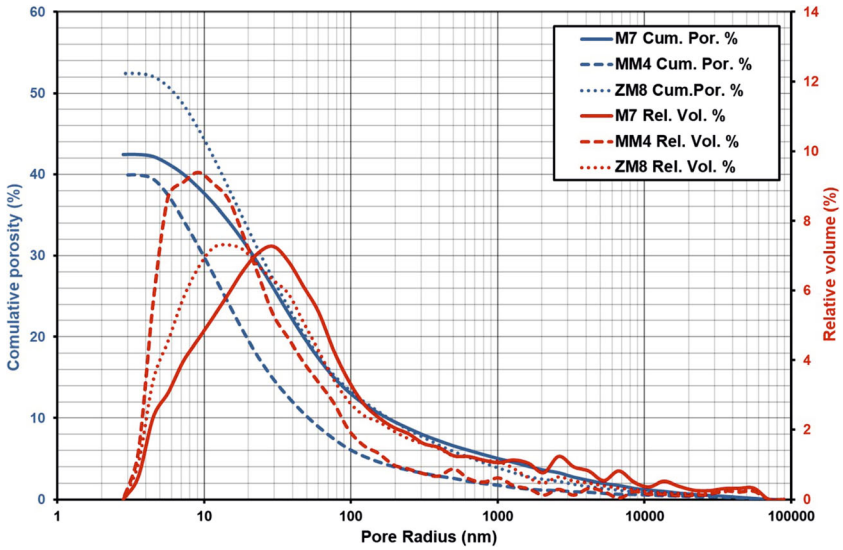

Fig. 12 Cumulative pore size and relative pore size distribution for M7, MM4 and ZM8 samples

SBW vs. CO_2 binary diagram (Fig. 11) classified all the investigated samples as natural pozzolanic mortars.

In addition, composition of the lime lumps confirms once again what the ancient texts stated. Pliny the Elder, in his *Naturalis Historia* (36), suggested that lime from white limestone is preferable; in particular, lime deriving from hard limestones (non-porous, and free from cracks; Brandon et al. 2014) turned to be more useful to produce concrete works (*structurae*), while lime deriving from porous stones works better for wall plaster and roofing; rocks containing flint is not recommended for both (Rispoli 2017). Stones extracted from quarries provide better lime than those taken on the banks of the rivers, and lime obtained from millstones is even better, due to its greasy quality (*Calcem e vario lapide Cato censorius inprobat; ex albo melior. Quae ex duro, structurae utilior; quae ex fistuloso, tectoriis; ad utrumque damnatur ex silice. Utilior eadem effosso lapide quam ex ripis fluminum collecto, utilior e molari, quia est quaedam pinguior natura eius*).

As far as provenance of raw materials is concerned, the minero-petrographic and chemical analyses, along with the surrounding geological setting, confirmed a local origin. Volcanic fragments were ascribed to NYT formation (de Gennaro et al. 1999; Colella et al. 2017) due to their typical association: phillipsite > chabazite > analcime. Chemical analysis of pumice fragments also suggested a clear affinity with NYT.

Regarding ceramic fragments, it was quite hard to define their provenance due to the extreme differences among samples, and their use likely suggested recycling of building materials. The relevant role played by ceramic fragments was to provide hydraulicity to the mortars, as pointed out by HI evaluation (Fig. 7). Actually, coating mortars, containing both *pozzolana* and ceramics, are characterized by the highest HI

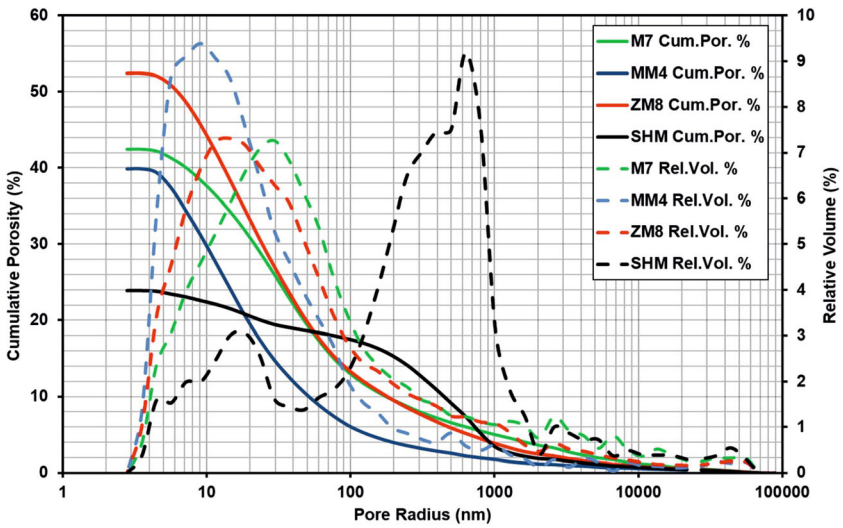

Fig. 13 Cumulative and relative pore size distribution in *Piscina Mirabilis* mortars (M7; MM4; ZM8) compared with standard hydraulic mortar (SHM)

values. The provenance of carbonate rocks used to produce lime for the investigated materials is still unknown, even if it is highly reasonable to assess that they were produced on site from carbonate deposits of Mesozoic age that border Campanian plain (Fig. 2). As regards secondary minerogenetic processes, composition of cementiceous-binding matrix is extremely intriguing. In fact, the association of C-A-S-H phase, calcite, gypsum and Al-tobermorite was noticed. C-A-S-H gel as previously said derived from pozzolanic reaction between lime and volcanic and ceramic aggregates; usually, calcite is related to unreacted clasts of underburned lime. Nonetheless, carbonation processes of residual portlandite may not be excluded; gypsum, the main newly formed mineral, is related to calcite sulphation by atmospheric SO_2 (de Gennaro et al. 1993). Al-tobermorite, an unusual hydrotermal, calcium-silicate hydrate mineral with cation exchange properties (Jackson et al. 2017), was unexpectedly retrieved in relict voids of *Piscina Mirabilis* mortars. Generally, Al-tobermorite synthesizes at 120–240 °C (Jackson et al. 2017), but these temperatures are incompatible with those of lime-based materials (Collepardi et al. 2009; Rispoli et al. 2015). According to Jackson et al. (2017), Al-tobermorite crystallization in Roman concretes at low temperatures could be linked to the concomitant occurrence of zeolitized products. Actually, lime mortars, mixed with zeolitized materials (a typical recipe of Roman engineers), react with seawater forming a highly alkaline, but relatively short-lived pozzolanic system buffered by calcium hydroxide, which produced C-A-S-H phase and Al-tobermorite at temperature < 95 °C (Jackson et al. 2017). This suggested the use of seawater to produce mortars used for building *Piscina Mirabilis*.

Finally, results of porosity tests together with microstructural observations highlighted that Piscina Mirabilis mortars have very small pore size radii (2.5–100 nm), about one order of magnitude lower than modern conventional mortars (100–1000 nm). These differences are probably due to the vesicular structure of pozzolanic materials (i.e. pumice) that represents a fundamental feature of the complex pore structure of the cementitious matrix of ancient mortars. Secondary minerogenetic products (Al-tobermorite and C-A-S-H gel) fill the pores enhancing bonding of pumice clasts and leading low permeability and a slow fluid diffusion through mortars over time, providing a relatively stable chemical system (Brandon et al. 2014; Jackson et al. 2017).

Conclusions

This research, further than representing the first mineropetrographic characterisation of mortars from one of the most important archaeological sites of *Campi Flegrei* (*Piscina Mirabilis*), shed new light on the provenance of raw materials and provided further information on the technology used for the preparation of such a revolutionary building material created by ancient Romans.

- Raw materials had a local provenance as they are well consistent with the surrounding geological setting. Pozzolanic materials represented by volcanic fragments, scoriae, pumiceous and crystal fragments deriving from pyroclastic rocks of the CFA are the most important components of the Roman recipe for hydraulic mortars. The addition of ceramic fragments in coating mortars further improved the pozzolanic attitude. It was not possible to define provenance of this ceramic aggregate due to strong differences among samples (e.g. recycling of fictile materials).
- A common feature of the investigated mortars is the high hydraulicity, which is also shown by the reaction rims around the pozzolanic materials. Such a feature is the result of an accurate selection, preparation and mixing of geomaterials, supplied by the geological availability of the area surrounding the archaeological site.
- Composition of cementitious binding matrix is peculiar as testified by different reaction products, including amorphous C-A-S-H gel, calcite and Al-tobermorite. In particular, this latter secondary minerogenetic product fills the pore spaces and enhances bonding in pumice clasts (Jackson et al. 2017). Formation of Al-tobermorite is also related to specific chemical elements (i.e. alkali cations) that, by contrast, in modern mortars and concretes generally produce unwanted expansion and corrosion of steel reinforcements (alkali-silica reaction, ASR), while in Roman mortars increase ductility and mechanical resistance (Jackson et al. 2017).
- The main difference between ancient Roman mortars and modern hydraulic mortars (SHM) is related to porosity. Despite of a total higher porosity, Roman mortars show much finer pores (between 4 and 120 nm) if compared with SHM (up to 1000 nm). Likely, such a different pore distribution positively affects the chemical and mechanical durability of Roman mortars, especially of those set along beaches and intertidal environments, where a continuous cycling of subaerial drying and moisture, and repetitive penetration of seawater salts into the mortars fabric take place (Brandon et al. 2014). Total volume and connectivity of pores in modern cementitious materials have important relapses on fluids pathways through mortar and/or concrete. Therefore, comparisons of pore features of ancient materials with conventional modern mortars might have a fundamental role to understand the excellent resistance to decay of ancient Roman concrete.
- This research contributes to the knowledge and understanding of technical skills achieved by ancient Romans and how their manufacturing technology was oriented to

innovation, quality, sustainability, durability and beauty. This study may also represent a valuable reference for future restoration projects of the investigated archaeological sites.

Acknowledgements This paper stem from the doctoral thesis of one of the Authors (CR) in earth science, environment and resources at DiSTAR of Federico II University of Naples. The authors would like to thank Dr. Roberto de Gennaro for the invaluable assistance during EDS microanalyses, Dr. Sergio Bravi for his technical ability in thin sections preparation and Dr. Pierfrancesco Talamo, former *Soprintendenza per i Beni Archeologici della Campania* that provided authorisation and useful support on sampling. Thanks are also due to CTG Italcementi Heidelberg Group for supporting this research activity. The authors would like to thank the journal editors and the anonymous reviewers for their useful comments that helped us in the revision of this manuscript.

References

Amalfitano P, Comodeca G, Medri M. (1990) I Campi Flegrei, un itinerario archeologico. Venezia

ASTM D4404–10:Standard test method for determination of pore volume and pore volume distribution of soil and rock by mercury intrusion porosimetry

Bakolas A, Biscontin G, Contardi V, Francesehi E, Moropoulou A, Palazzi D, Zendri E (1995) Thermoanalytical research on traditional mortars from Venice. Thermochim Acta 269/270:817–828

Barba L, Blancas J, Manzanilla LR, Ortiz A, Barca D, Crisci GM, Miriello D, Pecci A (2009) Provenance of the limestone used in Teotihuacan (Mexico): a methodological approach. Archaeometry 51:525–545

Belfiore CM, La Russa MF, Mazzoleni P, Pezzino A, Viccaro M (2010) Technological study of "ghiara" mortars from the historical city centre of Catania (eastern Sicily, Italy) and petro-chemical characterisation of raw materials. Environ Earth Sci 61:995–1003. https://doi.org/10.1007/s12665-009-0418-5

Borriello M. and D'Ambrosio A. (1979) Baiae-Misenum, Forma Italiae, Regio I, Vol. XIV. Firenze.

Boynton R. S. (1996) Chemistry and technology of lime and limestone. John Wiley & Sons.

Brandon CJ, Hohlfelder RL, Jackson MD, Oleson JP (2014) Building for eternity. The history and technology of roman concrete engineering in the sea. Oxford: Oxbow Books.

Colella A, Di Benedetto C, Calcaterra D, Cappelletti P, D'Amore M, Di Martire D, Graziano SF, Papa L, de Gennaro M, Langella A (2017) The neapolitan yellow tuff: an outstanding example of heterogeneity. Constr Build Mater 136:361–373

Collepardi M (2003) La lezione dei romani: durabilità e sostenibilità delle opere architettoniche e strutturali. In: III Convegno AIMAT "Restauro e Conservazione dei Beni Culturali: Materiali e Tecniche." Cassino (FR)

Collepardi M, Collepardi S, Troli R (2009) Il nuovo calcestruzzo, 5th edn. Treviso

De Feo G, De Gisi S, Malvano C, De Biase O (2010) The greatest water reservoirs in the ancient Roman world and the "Piscina Mirabilis" in Misenum. Water Sci Technol Water Supply 10:350–358. https://doi.org/10.2166/ws.2010.106

de Gennaro M, Colella C, Pansini M (1993) Hydrothermal conversion of trachytic glass into zeolite. II reactions with high-salinity waters. Neues Jahrb Far Mineral 3:97–110

de Gennaro M, Incoronato A, Mastrolorenzo G, Adabbo M, Spina G (1999) Depositional mechanisms and alteration processes in different types of pyroclastic deposits from Campi Flegrei volcanic field (Southern Italy). J Volcanol Geotherm Res 91:303–320. https://doi.org/10.1016/S0377-0273(99)00040-2

de Gennaro M, Cappelletti P, Langella A, Perrotta A, Scarpati C (2000) Genesis of zeolites in the neapolitan yellow tuff: geological, volcanological and mineralogical evidence. Contrib Mineral Petrol 139: 17–35. https://doi.org/10.1007/s004100050571

De Luca R, Miriello D, Pecci A, Dominguez-Bella S, Bernal-Casasola D, Cottica D, Bloise A, Crisci GM (2015) Archaeometric study of mortars from the Garum shop at Pompeii, Campania, Italy. Geoarchaeology 30:330–351. https://doi.org/10.1002/gea.21515

Deino AL, Orsi G, de Vita S, Piochi M (2004) The age of the neapolitan yellow tuff caldera-forming eruption (Campi Flegrei caldera-Italy) assessed by $^{40}Ar/^{39}Ar$ dating method. J Volcanol Geotherm Res 133: 157–170. https://doi.org/10.1016/S0377-0273(03)00396-2

Delile H, Keenan-Jones D, Blichert-Toft J, Goiran JP, Arnaud-Godet F, Romano P, Albarède F (2016) Urban development in ancient Naples. Proc Natl Acad Sci. https://doi.org/10.1073/pnas.1600893113

Di Benedetto C, Cappelletti P, Favaro M, Graziano SF, Langella A, Calcaterra D, Colella A (2015) Porosity as key factor in the durability of two historical building stones: neapolitan yellow tuff and vicenza stone. Eng Geol 193:310–319. https://doi.org/10.1016/j.enggeo.2015.05.006

Di Benedetto C, Graziano SF, Guarino V, Rispoli C, Munzi P, Morra V, Cappelletti P (2018) Romans' established skills: mortars from D46b mausoleum, Porta Mediana necropolis, Cuma (Naples). Mediter Archaeol Archaeom 18:131–146. https://doi.org/10.5281/zenodo.1285895

Fedele L, Scarpati C, Lanphere M, Melluso L, Morra V, Perrotta A, Ricci G (2008) The breccia museo formation, Campi Flegrei, Southern Italy: geochronology, chemostratigraphy and relationship with the Campanian Ignimbrite eruption. Bull Volcanol 70:1189–1219. https://doi.org/10.1007/s00445-008-0197-y

Fedele L, Insinga DD, Calvert AT, Morra V, Perrotta A, Scarpati C (2011) 40Ar/39Ar dating of tuff vents in the Campi Flegrei caldera (Southern Italy): toward a new chronostratigraphic reconstruction of the Holocene volcanic activity. Bull Volcanol 73:1323–1336

Fernández R, Nebreda B, De La Villa RV, García R, Frías M (2010) Mineralogical and chemical evolution of hydrated phases in the pozzolanic reaction of calcined paper sludge. Cem Concr Compos 32:775–782. https://doi.org/10.1016/j.cemconcomp.2010.08.003

Fichera GV, Belfiore CM, La Russa MF, Ruffolo SA, Barca D, Frontoni R, Galli G, Pezzino A (2015) Limestone provenance in roman lime-volcanic ash mortars from the Villa dei Quintili, Rome. Geoarchaeology 30:79–99. https://doi.org/10.1002/gea.21504

Gotti E, Oleson JP, Bottalico L, Brandon C, Cucitore R, Hohlfelder RL (2008) A comparison of the chemical and engineering characteristics of ancient roman hydraulic concrete with a modern reproduction of vitruvian hydraulic concrete. Archaeometry 50:576–590. https://doi.org/10.1111/j.1475-4754.2007.00371.x

Graziano SF, Di Benedetto C, Guarino V, Rispoli C, Munzi P, Morra V, Cappelletti P (2018) Technology and building materials in Roman age (1st BC-2nd AD): the "Mausoleo Della Sfinge" from the archaeological site of Cuma (Italy). Mediter Archaeol Archaeom 18:81–94. https://doi.org/10.5281/zenodo.1256057

Howarth J (1998) Improved estimators of uncertainty in proportions, point-counting, and pass-fail test results. Am J Sci 298:594–607

Izzo F, Arizzi A, Cappelletti P, Cultrone G, De Bonis A, Germinario C, Graziano SF, Grifa C, Guarino V, Mercurio M, Morra V, Langella A (2016) The art of building in the Roman period (89 B.C.-79 a.D.):

mortars, plasters and mosaic floors from ancient Stabiae (Naples, Italy). Constr Build Mater 117:129–143. https://doi.org/10.1016/j.conbuildmat.2016.04.101

Izzo F, Grifa C, Germinario C, Mercurio M, De Bonis A, Tomay L, Langella A (2018) Production technology of mortar-based building materials from the arch of Trajan and the Roman theatre in Benevento, Italy. Eur Phys J Plus 133. https://doi.org/10.1140/epjp/i2018-12229-1

Jackson M, Marra F (2006) Roman stone masonry: volcanic foundations of the ancient city. Am J Archaeol 110:403–436. https://doi.org/10.3764/aja.110.3.403

Jackson MD, Chae SR, Mulcahy SR, Taylor R, Li P, Emwas A, Moon J, Yoon S, Vola G, Wenk H, Monteiro P (2012) Unlocking the secrets of Al-tobermorite in Roman seawater concrete. Am Mineral 98: 1669–1687. https://doi.org/10.2138/am.2013.4484

Jackson MD, Gudmundsson MT, Bach W, Cappelletti P, Coleman NJ, Ivarsson M, Jónasson K, Jørgensen SL, Marteinsson V, McPhie J, Moore JG, Nielson D, Rhodes JM, Rispoli C, Schiffman P, Stefánsson A, Türke A, Vanorio T, Weisenberger TB, White JDL, Zierenberg R, Zimanowski B (2015) Time-lapse characterization of hydrothermal seawater and microbial interactions with basaltic tephra at Surtsey volcano. Sci Drill 20. https://doi.org/10.5194/sd-20-51-2015

Jackson MD, Mulcahy SR, Chen H, Yao L, Qinfei L, Cappelletti P, Rudolf H (2017) Phillipsite and Al-tobermorite mineral cements produced through low-temperature water-rock reactions in Roman marine concrete. Am Mineral 102:1435–1450. https://doi.org/10.2138/am-2017-5993CCBY

La Russa MF, Ruffolo SA, Ricca M, Rovella N, Comite V, De Buergo MA, Crisci GM, Barca D (2015) Archaeometric approach for the study of mortars from the underwater archaeological site of Baia (Naples) Italy: preliminary results. Period di Mineral 84:553–567. https://doi.org/10.2451/2015PM0031

Langella A, Bish DL, Cappelletti P, Cerri G, Colella A, de Gennaro R, Graziano SF, Perrotta A, Scarpati C, de Gennaro M (2013) New insights into the mineralogical facies distribution of Campanian Ignimbrite, a relevant Italian industrial material. Appl Clay Sci 72: 55–73. https://doi.org/10.1016/j.clay.2013.01.008

Le Bas MJ, Le Maitre RW, Streckeisen A, Zanettin B (1986) A chemical classification of volcanic rocks based on the total alkali-silica diagram. J Petrol 27:745–750

Mays L, Antoniou GP, Angelakis AN (2013) History of water cisterns: legacies and lessons. Water 5:1916–1940. https://doi.org/10.3390/w5041916

Melluso L, de'Gennaro R, Fedele L, Franciosi L, Morra V (2012) Evidence of crystallization in residual, Cl-F-rich, agpaitic, trachyphonolitic magmas and primitive Mg-rich basalt-trachyphonolite interaction in the lava domes of the Phlegrean fields (Italy). Geol Mag 149:532–550. https://doi.org/10.1017/S0016756811000902

Moropoulou A, Bakolas A, Bisbikou K (1995) Characterization of ancient, byzantine and later historic mortars by thermal and X-ray diffraction techniques. Thermochim Acta 269–270:779–795. https://doi.org/10.1016/0040-6031(95)02571-5

Moropoulou A, Cakmak A, Labropoulos KC, Van Grieken R, Torfs K (2004) Accelerated microstructural evolution of a calcium-silicate-hydrate (C-S-H) phase in pozzolanic pastes using fine siliceous sources: comparison with historic pozzolanic mortars. Cem Concr Res 34:1–6. https://doi.org/10.1016/S0008-8846(03)00187-X

Moropoulou A, Bakolas A, Anagnostopoulou S (2005) Composite materials in ancient structures. Cem Concr Compos 27:295–300. https://doi.org/10.1016/j.cemconcomp.2004.02.018

Morra V, Calcaterra D, Cappelletti P, Colella A, Fedele L, de Gennaro R, Langella A, Mercurio M, de Gennaro M (2010) Urban geology: relationships between geological setting and architectural heritage of the Neapolitan area. J Virtual Explor 36. https://doi.org/10.3809/jvirtex.2010.00261

Munsell Color (1994). Munsell Soil Color Charts (1994). Rev. edn. Macbeth Division of Kollmorgen Instruments, New Windsor, NY

Rispoli C. (2017) Ancient Roman mortars: mix design, mineralogical composition and minerogenetic secondary processes. Ph.D. Thesis, Federico II University of Naples, Naples, Italy

Rispoli C, Graziano SF, De Bonis A, Cappelletti P, Esposito R, Talamo P (2015) Piscina Mirabilis: characterization of geomaterials. In: 1st International Conference on Metrology for Archaeology. Benevento, pp 266–270

Rispoli C, Graziano SF, Guarino V, De Bonis A, Di Benedetto C, Esposito R, Budetta T, Morra V, Cappelletti P (2016) Characterization of ancient mortars: preliminary results from *Villa del Pezzolo*, Sorrento Peninsula, Italy. In: IMEKO International Conference on Metrology for Archeology and Cultural Heritage, MetroArcheo 2016. pp 151–156

Rispoli C, Fedele L, Di Benedetto C, Esposito R, Graziano SF, Guarino V, Morra V, Cappelletti P (2019a) Characterization of building materials from the Anfiteatro Flavio (Pozzuoli, Southern Italy): a mineralogical and petrographic study. Ital J Geosci 138:103–115. https://doi.org/10.3301/IJG.2018.29

Rispoli C, De Bonis A, Guarino V, Graziano SF, Di Benedetto C, Esposito R, Morra V, Cappelletti P (2019b) The ancient pozzolanic mortars of the thermal complex of Baia (Campi Flegrei, Italy). J Cult Herit, ISSN 1296–2074. https://doi.org/10.1016/j.culher.2019.05.010

Scarpati C, Cole P, Perrotta A (1993) The neapolitan yellow tuff-a large volume multiphase eruption from Campi Flegrei, Southern Italy. Bull Volcanol 55:343–356. https://doi.org/10.1007/BF00301145

Silva DA, Wenk HR, Monteiro PJM (2005) Comparative investigation of mortars from Roman colosseum and cistern. Thermochim Acta 438: 35–40. https://doi.org/10.1016/j.tca.2005.03.003

Stanislao C, Rispoli C, Vola G, Cappelletti P, Morra V, de Gennaro M (2011) Contribution to the knowledge of ancient Roman seawater concretes: Phlegrean pozzolan adopted in the construction of the harbour at Soli-Pompeiopolis (Mersin, Turkey). Period di Mineral 80:471–488. https://doi.org/10.2451/2011PM0031

UNI-EN 11305:2009 Beni culturali: Malte storiche, linee guida per la caratterizzazione mineralogico petrografica, fisica e chimica delle malte

UNI-EN 196-1:2005 Methods of testing cement-Part 1: Determination of strength

UNI-EN 197-1:2011 Cemento-Parte 1: Compopsizione, specificicazioni e criteri di conformità per cementi comuni

Whitney DL, Evans BW (2010) Abbreviations for names of rock-forming minerals. Am Mineral:185–187

Zawawi R (2006) Artificial hydraulic lime mortar obtained by calcining limestone and siliceous waste materials. J Adv Appl Ceram 10:175–178